1.2. Regularities of sea ice formation depending on hydrological and meteorological conditions

Hydrometeorological processes, which cause changes of sea ice amount, are divided into *thermal* and *dynamic* by nature of influence. Effect of thermal processes leads to increasing or decreasing of ice amount by means of aggregative transformation water↔ice (ice growth and melting), and also can lead to changes of salinity and heat content of surrounding waters. Due to this heat content and salinity in ambient water changes. Effect of dynamic processes can lead to ice mass redistribution in any water area as the result of increasing concentration, diverging and ice hummocking. Ice mass also changes due to ice exchange with neighbor water areas. Thus, these types of processes cause changes of ice balance both in the unit of region, and in entire sea.

1.2.1. Thermal processes in ice cover of the Arctic Seas

Thermal processes have essential features in spring-summer and autumn-winter periods. Mathematical description of these processes differs respectively.

1.2.1.1. Features of thermal processes in spring-summer period

The most significant process if this period is ice melting. Ice area and mass decrease in the vast water areas of the Arctic Seas. It directly influences terms of fast ice melting, values of ice cover and ice massifs area, changes of distribution of ice concentration.

Ice melting occurs as a result of ice cover heat absorption, coming from different sources (Fig. 1.2.1.). Combined influence of this heat on ice cover can be expressed by heat balance equation:

$$\frac{\partial m}{\partial t} = \frac{1}{\rho_л L}(R + \Phi + D - W_{mc}), \qquad (2.1.1)$$

where R – total heat flow, caused by radiation processes;

Φ – total heat flow, caused by turbulent processes; D – total heat flow, caused by advection processes;

Wтс – part of total heat flow, which changes ice temperature;

In equation (2.1) $R=Q_{пр}+Q_р-Q_{отр}+E_а-E_л$,

Where: Q –short-wave component of solar radiation$Q_{пр}$– direct,

$Q_р$ – diffused,

$Q_{отр}$– reflected of its parts (sum $Q_{пр}+Q_р=Q_{сум}$ is called total radiation, and $Q_{пр}+Q_р–Q_{отр}= Q_п$ – incident radiation; E – long-wave component

$E_л$ – ice cover radiation,

E_a –counter radiation of atmosphere ($E_л – E_a = E_{эф}$ – effective radiation).

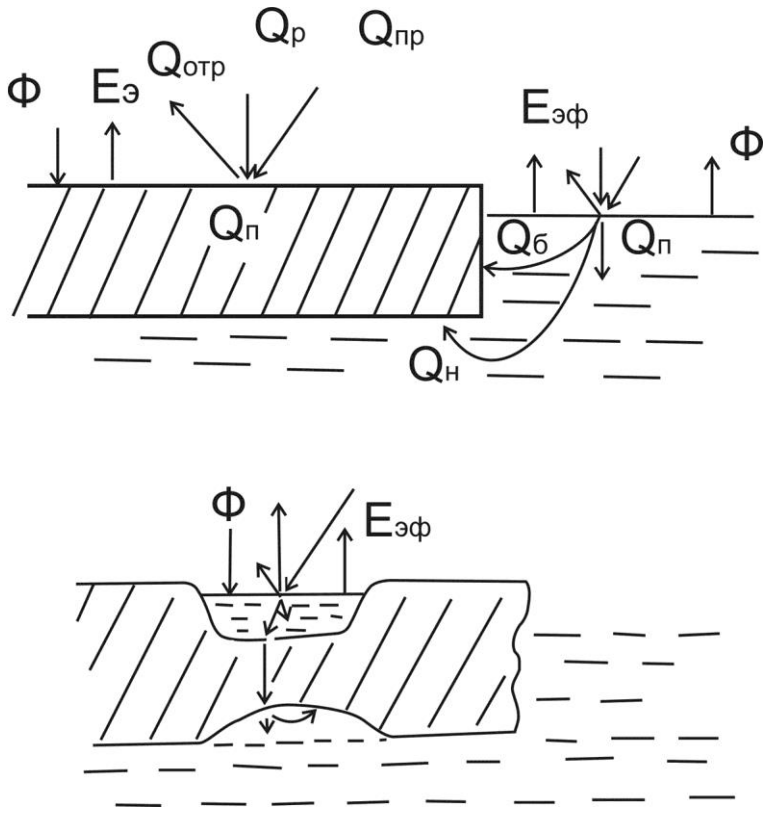

Fig. 1.2.1 – Scheme of ice cover heat balance components in summer

Turbulent processes are in effect both in atmosphere ($Φ_a$), and in water ($Φ_w$). The first ones have two components, one of which is determined by heat exchange, and the second is determined by moisture exchange, connected with changes of aggregate state water↔ vapour and ice↔ vapour.

Heat advection (D) in sea and atmosphere is significant within limited areas, where horizontal gradients of temperature (near ice edge) and current's velocity are high. On the larger part of the Arctic Seas this component, as well as $W_{тс}$ value can be neglected in ice melting calculations.

Main features of other components of heat balance in spring-summer period are discussed.

Direct and diffused radiations depend on astronomical reasons (sun height above the horizon) and, thus, significantly change with latitude and during the year. Both components depend on cloudiness. However, if direct radiation decreases with the increase of cloudiness, diffused radiation, in contrary, increases. Due to this and due to small interannual variability of cloudiness in the Arctic in summer, interannual anomalies of total radiation are not large, and can be neglected in

calculation.

If $E_л$ and E_a are close in value, $E_{эф}$ is small, changing during the year from 1,0 – 1,5 ccal/cm^2 in summer to approxamately2 ccal/ cm^{2}month in winter. Interannual changes of these values don't normally exceed ±0,4 ccal/ cm^{2}month.

During May-September input part of heat balance exceeds its output. On average during this period $Q_п$ is approximately 16 ccal/ cm^2, that is enough for ice melting with thickness of 200 cm. It's the main heat source, spent on ice melting. Its interannual variability is mostly defined by albedo variability, because direct influence of cloudiness, moisture, ice ($T_л$) and temperature (T_a) variability can be neglected.

Turbulent fluxes of explicit and latent heat are proportional to difference $T_a – T_л$, at that proportional coefficients (Stanton and Dalton coefficients) depend on atmospheric stratification and wind velocity. Turbulent fluxes are normally large near coast and ice edge. In consequence of transformation T_a above melting ice (Fig. 1.2.2) with moving off the listed boundaries T_a rapidly approach to $T_л$, that is why direct role of turbulent fluxes on the upper ice surface and its interannual variability in ice melting is not large. However, they significantly influence ice melting indirectly, defining the moment, when ice melting starts, on which albedo changes in the following time depend on.

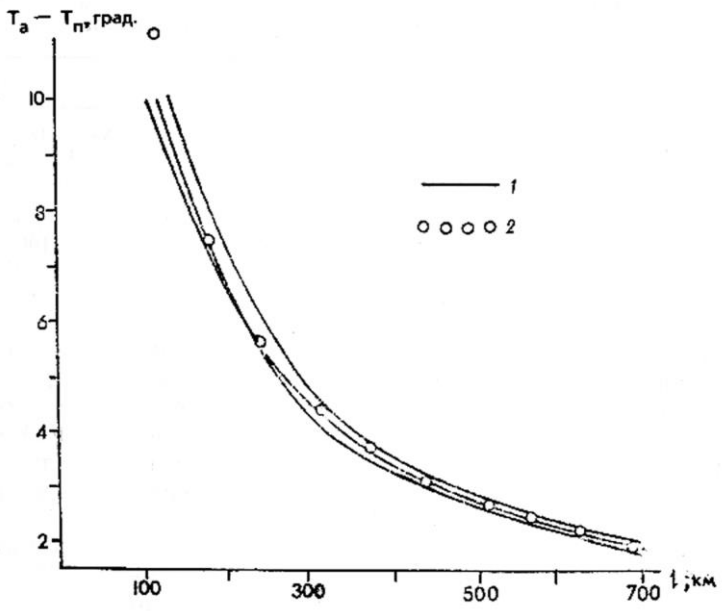

Fig. 1.2.2 – Changes of air temperature over ice cover in summer
1 –empirical curves; 2 – their approximation

Question about albedo value of melting ice – is one of the most important in melting calculation, as $Q_п = Q_{сум}(1 – A)$. Value A depends on ice cover decay, values T_a, of initial ice thickness, thickness of melted layer, snow depth, depth and area of puddles. Relative area of puddles on average increases from 5% in the end of the first decade from the beginning of melting

to 35% in the end of third decade, after that due to melt water filtration through ice it gradually decreases to 5% in the end of eights decade. Average area of puddles decreases with increasing hummocking and for smaller forms, and increases with reduction of ice thickness.

Simultaneous occurrence of several types of ice surface is typical for melting of ice cover. These are: snow cover, co-called dry ice zones and water surface of puddles and thaw holes. Reflectivity of these types is different. Gradual changes of radiative snow properties on average are characterized by albedo decreasing from 0,90 to 0,65. The last value is related to dry ice zones after snow cover disappearance. Further decreasing of albedo is caused by appearance and evolution of puddle area and depth (their reflectivity varies within limits of 0,10 – 0,40 depending on depth and pollution). Thus, when puddles are formed, which is close in time to ice melting beginning, albedo value and heat balance of snow-ice cover absolutely changes.

Solving equation of heat balance under condition $T_a=T_{нт}$, $T_п=0$, $\partial h/\partial t=0$, $D=W_{тс}=0$, is found from the following expression:

$$T_{нт}=\frac{0{,}25Q_{сум}-E_{эф}}{0\sigma 24v}+0{,}6 \qquad (1.2.2)$$

From equation (1.2.2) it is found, that the bigger is $Q_{сум}$ and the less is $E_{эф}$, the lower is $T_{нт}$: $-1{,}5< T_{нт}< 2^0C$.

At the moment, when $T_a=T_{нт}$, is term of melting beginning. From Fig. 1.2.3., on which the seasonal dependence of average and extreme air temperatures is compared to changes of $T_{нт}$, it is seen, that terms of melting beginning can vary from late May to early July.

On Fig. 1.2.4 annual mean dependence of decade values $Q_{сум}$, typical for the Arctic Seas is shown. Segment AB means period of probable terms of melting beginning. If melting begins in early terms, it'll cover period of maximum Qсум values and maximum amount of solar energy will be spend on it. If melting begins in late terms, this amount will decrease twice comparing to the early terms of melting beginning. Amount of melted ice and terms of ice destruction change correspondingly.

Besides terms of melting beginning, ice cover melting (destruction) and thickness of ice, which survived summer melting, also depends on initial thickness of ice and snow.

If taking into account only melting of upper ice surface and under average conditions, ice in the south-western Kara and Chukchi Seas completely melts away to the end of second decade of August, and in the eastern East-Siberian Sea - to the middle of first decade of September.

In the other Arctic Sea regions ice doesn't completely melt away, and thickness of ice, which survived summer melting, is about 50 cm in the western East-Siberian Sea, about 60 cm in the

eastern Laptev Sea and about 100 cm in its western region and the north-eastern Kara Sea.

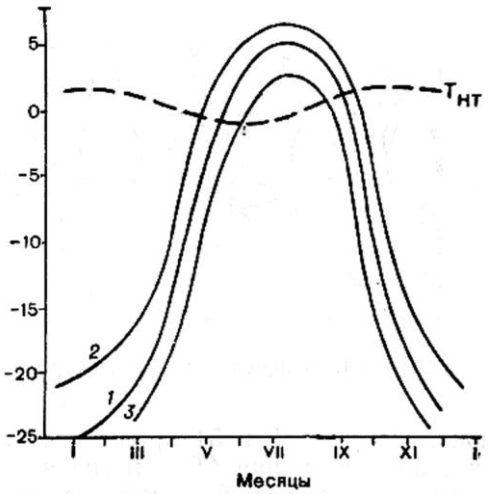

Fig. 1.2.3 – Seasonal dependence of average (1) and extreme (2,3) air temperatures in the Arctic Seas; $T_{НТ}$ – temperature of melting beginning

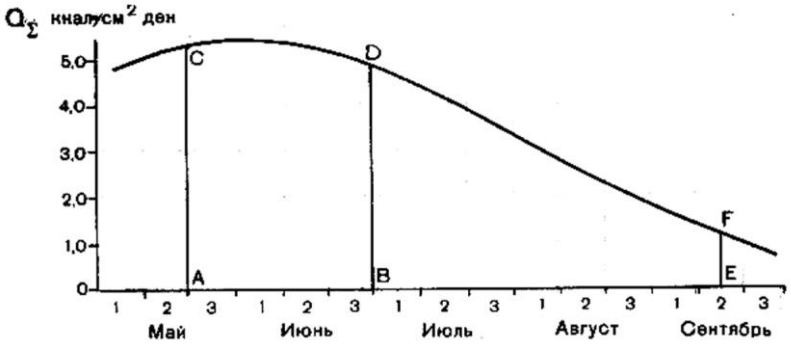

Fig. 1.2.4 – Annual mean dependence of 10-day mean values of total radiation in the Arctic Seas and terms of melting: A – earlier, B – later, E – end of melting

It is necessary to briefly consider special features of ice melting in puddles, which role in changes of ice cover albedo was shown before. Since attenuation of shortwave radiation in water (0,006 см$^{-1}$) is about 40 times less, than in ice, significant part of solar energy reaches puddle bottom and penetrates further to ice cover bottom. This fact not only facilitates rapid increase of puddle depth, but it also creates conditions for ice bottom melting. Thus, roughness is formed on this surface, which exactly reflects upper ice surface roughness. Another process, which accelerates ice melting processes on puddle bottom, is intensive convection in puddles, connected with increasing of strongly desalinated water density during its heating. All these processes cause transition of puddles into thaw holes, which facilitate increasing area of fractures under decay of ice fields, i.e. ice cover diverging.

Melt water mainly drains under ice through thaw holes, because water level in puddles before thaw holes formation is located above sea level, but lower than upper ice surface. Ice layer is often formed in zone of its contact with salt water under ice, which temperature is lower than freezing

point of strongly desalinated melt water. Under strong drift this ice breaks and floats to the surface as shuga, partly filling thaw holes and hollow space in ice keels.

Melting from above is not the only process of ice melting in summer period. Latent melting of ice floes and, partly, from bottom, due to heat absorption by fractures are also important. It is necessary to enumerate the following circumstances to characterize this process.

– Open water among ice absorbs 2 – 4 times more heat than ice cover surface;

– One part of this heat is spent on latent melting (concentration changes), another – to melting from bottom (thickness changes), the third – to water heating;

– Observations show, that water heat content in fractures is not large (3–4 ccal/cm^2); it increase, when fracture width increasing;

– The most reasonable suggestion was made by Yu.P. Doronin, is that part of heat absorbed in fractures ($Q_{пв}$), which is spent on latent melting ($Q_б$) and that from bottom ($Q_н$) is proportional to N (N – concentration of ice cover, expressed in tenths):

$$Q_б + Q_н = N \cdot Q_{пв} \qquad (1.2.3)$$

– Question about proportion of $Q_б/Q_н$ hasn't been solved;

– Role of $Q_б$ in ice melting increases, when ice thickness and ice concentration decrease; for average conditions in the Arctic Seas it is comparable with the role of melting from above, proportional to value $Q_п$.

Only insignificant part of heat is spent on water heating before ice disappearance. Thus, maximum value of heat content depends on terms of sea surface clearance from ice. In regions, where ice cover disappeared in early terms (May-June), maximum heat content (to 18ccal/ cm^2) is observed in late July-early August. Clearing terms influence insignificantly on maximum heating terms and its value. In contrary in regions, where ice cover disappears in late terms (July-August), terms of maximum heating change within limits of three decades, and its maximum value is up to 10 ccal/ cm^2. Area of open water is the reliable indicator of maximum sea heat content.

Maximum value of water heating depends on its density stratification (depth of active layer). The largest depth of active layer in summer period is registered in the Kara and Chukchi Seas (up to 25-30 m). In the Laptev and East-Siberian Seas depth of this layer doesn't normally exceed 10 m. However, observations show that part of heat penetrates into pycnocline layer, where it remains even after ice formation on the surface. Further, as a result of convection and turbulent heat exchange, this heat reaches ice bottom, reducing velocity of ice growth process. In regions, where stratification is feebly marked (most part of the Barents Sea), maximum content of heat in sea exceeds 50 ccal/ cm^2.

1.2.1.2. Peculiar Features of thermal processes in autumn-winter period

Main processes of autumn sea cooling, which in the Arctic Seas starts in late August – early September and lasts mainly during September-October, are: *effective radiation, turbulent heat exchange and evaporation* (approximately in equal parts). These fluxes in August-September are 0,5–2,5 ccal/cm^2, increasing in October-November up to 2,0–4,0 ccal/cm^2. Total effect of listed fluxes influence changes in space from less than 5 ccal/cm^2 in the Laptev and the East-Siberian Seas to 15 ccal/cm^2 in the western Kara Sea and in the central Chukchi Sea. Anomalies of heat loss are determined mostly by temperatures difference $T_a - T_w$, which normally depends on dominant wind direction.

Significant stage of ice growth process is its appearance on sea surface, free from ice cover. Following conditions have to occur on open sea surface to start stable ice formation: a) temperature of homogeneous surface water layer must decrease to water freezing point, taking into account this layer salinity; b) negative heat balance of water surface (by absolute value) must not be less than heat inflow to surface layer, caused by turbulent processes, convection and advection.

Nature of processes of heat exchange between atmosphere and sea significantly changes with the beginning of ice formation. Snow-ice cover, having high heat-insulating properties, becomes a factor, regulating this interaction. Effective radiation, which is directed from underlying surface to atmosphere during whole ice growth period due to large snow emissivity, is the main "term of expenditure" of snow-ice surface heat balance in winter period.

Turbulent fluxes Φ_a during first winter half are also directed from ice surface to atmosphere, but as soon as values T_a и $T_л$ become equal, they take the opposite direction.

Heat flux from ice bottom to its upper surface is itself sum of heat fluxes extracting on ice bottom under ice formation (latent crystallization heat), and heat, coming to ice bottom from underlying water layers as a result of turbulent and convectional mixing. This heat flux depends on heat-insulating properties of ice and snow. It increases with increase of temperature contrasts between lower and upper surfaces of ice cover, and decreases with ice thickening and snow height growth.

Estimations of heat fluxes, coming to ice bottom from water, significantly differ in works by different authors: above continental slope – from 4 to 6–8 ccal/cm^2, above deep-water Arctic basin – from 1,0 to 1,5–3,0 ccal/cm^2. Necessary to mention, that under influence of climate warming and corresponding strengthening of cyclonic activity above Arctic, not only temperature of deep Atlantic water increase, its upper boundary rise, but also salinity of upper mixed layer increase. As a result water stratification gets weaker, and heat flux from water column increases. Its changes

have to be reasonably estimated.

Large irregularity of ice cover thickness, different snow depth, and especially, occurrence of cracks, channels and leads cause irregularity in distribution of heat fluxes from underlying surface to atmosphere. In spite of rather small area of leads in compact ice cover, heat exchange with atmosphere through these formations is comparable with heat radiation of compact snow-ice cover.

Heat balance equation, similar to (1), can be used to calculate ice thickness changes in process of its growth, if substitute ice thickness H instead of ice mass m. However, accuracy of determination of components, consisting heat balance, is not high, because of their small value. Thus, other approach is used to determine ice thickness. So far as vertical heat flux through ice is proportional to ice heat conductivity λ and temperature gradient, and formed ice mass is proportional to crystallization heat L, heat balance equation on the ice-water boundary is given by:

$$L\rho\frac{\partial H}{\partial t} = \lambda\frac{\partial T}{\partial z} - F_w \qquad (1.2.4)$$

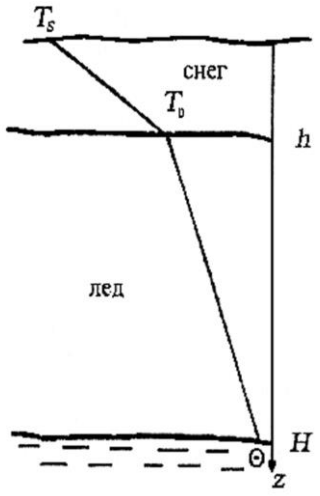

Fig. 1.2.5 – Temperature profiles for first-year ice - snow cover in winter

Expression (1.2.4) doesn't take into account almost permanent snow cover existing on ice surface, which influence ice thickness growth a lot. In order to allow for this influence, vertical temperature profile in ice and snow can be presented as broken line, coming through temperature values T_s, T_0 and Θ (Fig. 1.2.5). It means that vertical heat flux in both mediums doesn't change, and is defined by the following equation:

$$\lambda\frac{\Theta - T_0}{H} = \lambda_s\frac{T_0 - T_s}{h} \qquad (1.2.5)$$

where h, λ_s - snow depth and heat conductivity;

T_0, T_s – temperature of ice and snow surface;

Θ - water freezing point.

From formula (1.2.5) we can derive equation for temperature on the ice-snow boundary as:

$$T_0 = \frac{H\lambda_s T_s + h\lambda\Theta}{h\lambda + H\lambda_s} \qquad (1.2.6)$$

Exact solution of equation (1.2.4), taking into account (1.2.5) and (1.2.6), can't be obtained because real conditions of ice growth are complicated (inconstancy of vertical temperature gradient in ice, dependence of thermalphysic ice characteristics on temperature and salinity and etc.). Calculations using approximate formulas, obtained in some works, fit observational data. Under assumption that snow depth, and also thermalphysic characteristics of ice and snow are constant during temporal step, authors of work obtained the following formula for ice thickness calculating:

$$H = -(\frac{\lambda}{\lambda_s}h + \frac{F_w}{L\rho}\tau) + \sqrt{(\frac{\lambda}{\lambda_s}h + \frac{F_w}{L\rho}\tau)^2 + H_0^2 + \frac{2\lambda}{L\rho}(\Theta - T)\tau - \frac{2h\lambda}{\lambda_s}(\frac{F_w}{L\rho}\tau - H_0)} \qquad (1.2.7)$$

calculations using formula (1.2.7) are made by method of successive approximations, according to which ice thickness, calculated on the previous step with length τ, is entered to radicand

If put in formula (1.2.7) numeric values λ and λ_s, equal to 2,2 and 0,3 joule/msdegree respectively, and neglect heat flow from water (F_w), simple formula can be received:

After substituting numerical values λ and λ_s, equal to 2,2 and 0,3 joule/m·s·degree respectively, in formula (1.2.7) and neglecting heat fluxes from water (F_w), a simple formula is given by:

$$H = -7{,}0h + \sqrt{(7.0h + H_0)^2 + 0.00122(\Theta - T_s)\tau} \qquad (1.2.8)$$

Growth of multiyear ice and ice, survived summer melting, has its own peculiar features. During melting of ice cover, especially its lower layers, content of liquid phase increases. Puddles stay on ice surface till the beginning of freezing. As a result heat sources of phase transfer occur in ice thickness, distorting quasi-linear vertical temperature changes. Under these conditions equation (1.2.8) becomes incorrect. Freezing process of puddles and liquid phase in ice depth leads to significant (sometimes for 2-3 months) delay of ice freeze-up on ice bottom. This circumstance, and also additional snow accumulation in zone of freezing puddles facilitates increase of mesoscale ice thickness irregularity. More complicated models are developed at the moment, taking into account phase transitions inside ice layer, nonlinearity of its temperature heat conductivity and heat capacity changes, depending on salinity.

Formula (1.2.8) allows calculating ice thickness in case of calm growth in the Arctic Seas in any moment of autumn-winter season – till the moment, when maximum thickness has reached, and also calculating ice thickness, formed in different time in water free from ice as a result of drift.

Reduction of ice thickening velocity with increasing its thickness, determined by thermodynamic processes, leads to idea of "equilibrium thickness", understood as ice cover thickness, when winter ice growth is equal to summer melting. Equilibrium ice thickness and time of its reaching depend on climate conditions, especially on value of heat flux from water. According to calculations by Ivanov B.V. and Makshtas A.P., heat flux from water increasing from 2 to 8 watt/m^2 (from 1,5 to 6 ccal/cm^2), cause equilibrium ice thickness decreases from 6 to 2 m. Ice cover thickness of the Arctic Seas doesn't normally reach equilibrium thickness, because of drift and gradual ice outflow southwards.

1.2.2. Dynamic processes in ice cover

Being located on the boundary of dynamic environments – atmosphere and ocean – sea ice cover is constantly influenced by these environments, resulting in motion (drift) of ice formations. Ice cover regions, limited by area and connected with coast or sea bottom (fast ice, hummocked ice), are exceptions.

First systematical observations of ice drift, made by F. Nansen during transartcic expedition onboard *Fram* (1893–1896), allowed discovering, that ice drift in the Arctic Basin has two main components: wind component, closely connected with the local wind, and "non-wind", which doesn't depend on the local wind at the moment of observations. The first component is caused by stresses at the upper ice cover surface, determined by relative air motion (wind), and the second is determined by different interrelated factors, such as gradient currents, sea level tilts, tidal phenomena, etc.

Direct observations of currents and water masses and different indirect methods, based on correlation of data on resulted ice drift and wind, or atmosphere pressure gradient for particular time periods, can be used to separate these components.

1.2.2.1. Peculiar features of wind drift

Velocity dependence from wind and barriers (shore, fast ice) and following to isobaric drift law are features of wind drift.

Wind drift velocity linear depends on velocity of wind, which caused it with quotient of given velocities (co-called wind coefficient, k) on average close to 0,02. Direction of wind drift deviates

from wind direction to the right (in Northern hemisphere) on angle (α), on average close to 30^0. Expressions for projections of wind drift velocity (V_x, V_y) on Cartesian coordinate axis (x, y), connecting them with corresponding wind velocity projections (W_x , W_y), are given by:

$$\left.\begin{aligned} V_x &= k\,(W_x \cos\alpha + W_y \sin\alpha) \\ V_y &= k\,(W_y \cos\alpha - W_x \sin\alpha) \end{aligned}\right\} \qquad (1.2.9)$$

Wind component of drift follows rather rapid after wind changes: ice drift gets stable normally in 3-6 hours after occurrence of stable wind.

Wind coefficient k and angle α significantly change during the year: they increase from the end of winter to the middle of summer. Seasonal changes of value k are 50% of its average meaning, and changes α – 40%.

Barrier occurrence (coast, fast ice) significantly influences size and direction of wind drift (normal to shore component decreases with approaching to coast).

Law of isobaric drift by N.N. Zubov is given by:

$$V_в = K \cdot (\partial P/\partial n) \qquad (1.2.10)$$

Using known formulas for projections of geostrophic wind velocity on axis x, y, projections of wind drift velocity can be expressed through gradient components of atmosphere pressure:

$$\begin{aligned} V_x &= K\cos\beta\left(\frac{\partial P}{\partial y} + tg\beta\,\frac{\partial P}{\partial x}\right) \\ V_y &= K\cos\beta\left(\frac{\partial P}{\partial x} + tg\beta\,\frac{\partial P}{\partial y}\right) \end{aligned} \qquad (1.2.11)$$

Here $K=kk_1/\rho_a f$ – isobaric coefficient, ρ_a , f – air density and Coriolis parameter, k_1 – relation of geostrophic and surface wind velocities $\beta = \alpha + \gamma$ (γ – wind inclination from isobar).

Seasonal dependence of isobaric coefficient is similar to wind coefficient changes. Angle of wind ice drift velocity inclination from isobar in the middle of summer exceeds $+20^0$ and decreases to the end of winter to -5^0 .

Average values of isobaric coefficients in Arctic Seas are on 25–40% higher and angles of drift inclination from isobar on $5–10^0$ less, than in the Arctic Basin. These differences can be explained by smaller ice thickness in the Arctic Seas, and also by influence of barotropic gradient currents, which role must increase with the reducing of sea depth and coast approaching. It is necessary to

mention, that when ice thickness is less than 100–120 cm, and in non-stationary conditions, angle β can take negative values with wind change not only in winter, but also in summer, which has the principal importance in processes of ice cover diverging, increasing its concentration and compacting.

1.2.2.2. Peculiar features of gradient currents influence on ice drift

The Role of gradient currents (together with tilt of level surface) in general ice drift of the Arctic Basin accounts for around 60% on average, increasing to 70%, when the ice approaches "Fram" Straight and to 90% in the Greenland Sea at latitude 74–78^0 N.

System of gradient currents in the Arctic Ocean (AO) is formed under influence of the following factors:

- Large-scale wind fields, determined by atmospheric circulation behavior;
- Fresh water balance of AO with its main components - river run off and overbalance of atmospheric precipitation over evaporation;
- Irregularity of water density distribution, conditional by mechanic and non-mechanic factors;
- Global inclination of level surface between the Atlantic and the Pacific Oceans;
- Water exchange conditions with neighbor oceans;
- AO morphologic features (shore configuration, bottom relief).

Effects of listed factors are closely connected with each other. At that wind fields influence on gradient currents system is affected as a result of adaptation of water mass field (water density) to resultant wind circulation. Thus, currents system in deep waters of AO is mostly baroclinic. A good stability of considered currents system is connected with this circumstance.

According to known schemes of gradient currents, large anticyclonic water circulation is located in the Amerasian subbasin, where anti cyclonic wind field dominates. On its periphery is located wide Transarctic current, which originates from the Pacific current of the Chukchi Sea and outflows from the Arctic Basin through Fram Straight. Its continuation in the Greenland Sea is the Eastern-Greenland current. In straights of the Canadian Arctic archipelago motion of surface waters is directed from the Arctic Basin to the Baffin Sea, where Labrador Current begins from. Average velocity of Transarctic current, approaching to Fram Straight, increase from 1–2 cm/s to 5–7 cm/s (in the straight) and to 18 cm/s (on latitude 72^{0}N in the Greenland Sea).

Current velocity changes during the year: in the Arctic Basin it is maximum in summer and minimum in winter, at that in addition to annual half annual component is also noticeable in these changes – according to seasonal changes of water inflow through Bering Straight. Winter maximum of current velocity, caused by appropriate changes of dominant wind, appears in seasonal changes in Fram Straight.

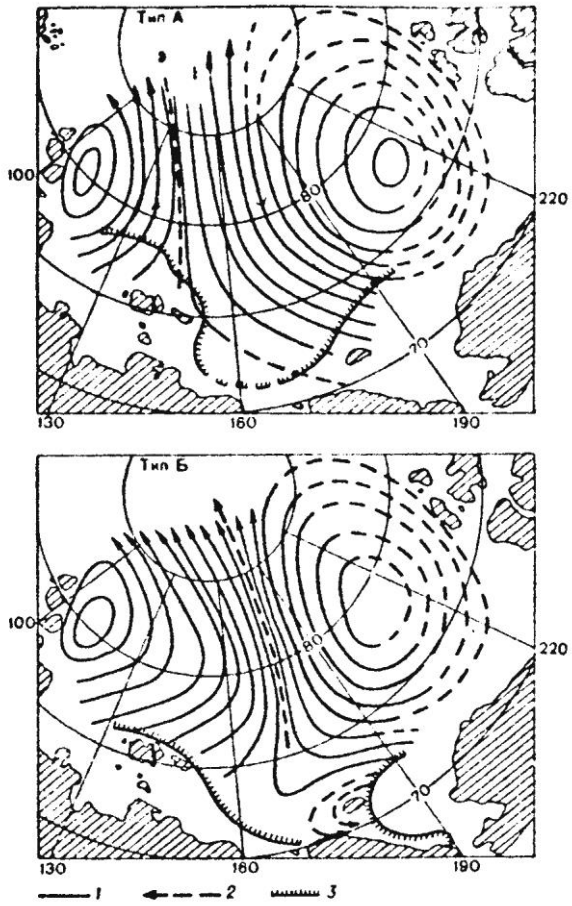

Fig. 1.2.6 – Typical dynamic maps of surface currents relative to horizon of 200: anticyclonic type (above) and cyclonic (bottom). 1 – lines of equal dynamic heights (through 20 din. mm), 2 – location of Transarctic current deep stream, 3 – average location of ice edge in August.

Oceanological surveys of the Arctic Basin, made in different years in high latitude airborne "Sever" expeditions, allowed discovering annual changes in surface current system (Fig. 1.2.6.). They are connected, firstly, with relation between areas of cyclonic and non-cyclonic circulation systems, and also with location of Transarctic current deep stream. Cyclicity with a period of 8-10 years was found in these changes. Ice conditions in the Arctic Seas, ice outflow to the Greenland Sea, inflow of Pacific waters and other indicators of hydrologic AO regime change in the same rhythms with them. Intensification of the Arctic anticyclone and its displacement to Eurasia lead to widening of anticyclonic circulation and shrinking of cyclonic. Weakening of anticyclone and its motion to American continent lead to opposite consequences. It is typical, that occurrence of similar changes in atmospheric circulation and corresponding system of barotropic currents in the Arctic Basin was confirmed in recent studies, where it was called "Arctic oscillation".

In the shallow Arctic Seas, especially near coast, distribution of water density doesn't reflect in full measure gradient currents structure and corresponding sea surface inclinations. Gradient

currents here are significantly barotropic. As formation time in such currents is rather short, gradient component of current, and consequently, of ice drift, correlates with wind well, being changed with the change of last one. This causes increase of empirically determined average values of wind coefficients, and their dependence on wind direction relative to coast.

In some regions of the Arctic Basin, especially in marginal seas, tidal currents significantly influence on ice drift, leading to appearance of ice drift periodic tidal component. Short-term (diurnal, semi-diurnal) and long-term (from several days to several years) tidal currents components (ice drift) are distinguished.

According to research data, direction and velocity of short-term component of tidal ice drift and tidal near surface currents practically coincide in every moment. Maximum velocity of semi-diurnal tidal currents on the large part of the Arctic Seas is 10–30 cm/s. Only in several limited areas it exceeds 1 cm/s. Maximum velocity of tidal ice drift in deep waters of the Arctic Basin doesn't normally exceed 5 cm/s. In quadrature it is 2–2,5 times less that in syzygy.

Trajectories of tidal ice drift are close to circle in most regions. Usually they are reversible only near a coast. Estimations, based on long wave's theory, show that in the most regions of the Arctic Seas maximum ice displacement by tidal wave is 2-4 km, rarely reaching 20 km, whereas in the Arctic Basin it doesn't normally exceed 1 km. However, practical importance of tidal ice drift is caused by significant spatial irregularity of its velocity, connected with increasing sea ice concentration, diverging and compacting. Tidal currents are important in process of fast ice formation.

Apart from tidal motion ice drift is affected by inertial oscillations in horizontal plane. They lead to appearance of folded trajectories with radius, depending on initial drift velocity and latitude. In the Arctic Seas, where the period of inertial oscillations is close to period of main tidal semi-diurnal waves, a radius of inertial orbits is normally about 1 km. It is rather difficult to separate inertial and tidal ice motion. Long-term and accurate observations are obligatory for this purpose.

1.2.2.3. Total ice drift in the Arctic Basin

Average velocities of total ice drift and characteristics of its variability strongly depend on time scale: if averaging period increases, average velocity of ice drift decreases from 7,5 cm/s to 2,2 cm/s for daily and annual periods respectively, i.e. almost 3,5 times. Statistical characteristics of ice drift velocity have annual variations. As seen from Fig. 1.2.7, average ice drift velocity modules for daily, 10-day and monthly periods vary within a year concordantly: the smallest mean drift velocities are observed in March, and the largest ones – at the end of summer – beginning of autumn (August-October). However, average velocity modules change little over 3-month period

throughout the year and become practically equal for 6-month periods, since seasonal velocity increase is compensated, by the end of summer, by its decreasing stability.

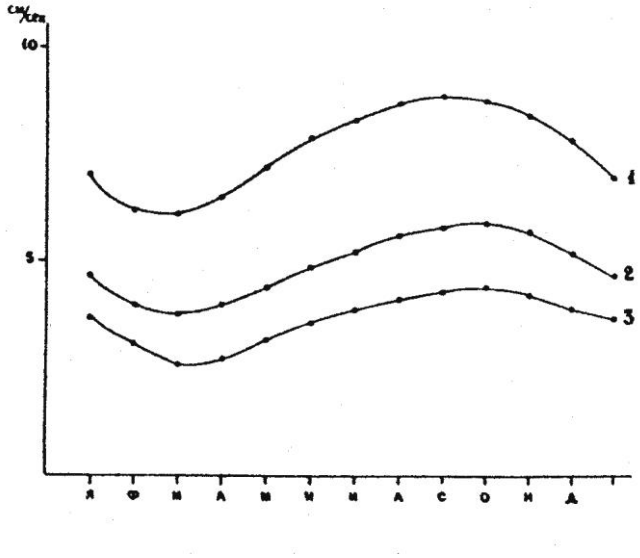

Fig. 1.2.7 – Annual dependence of average module of ice drift for dayly (1), 10-day (2) and monthly (3) periods

Schemes of average resultant ice drift in the Arctic Basin for winter and summer half years, calculated from observational data of drifting expeditions and automatic buoys, using drift field approximation by two-dimensional polynominals in cube, are shown in Fig. 1.2.8 (a,b)

$$V_i = \sum_{q=0}^{t} \sum_{p=0}^{m} \left(a_{pq}\right)_i X^p Y^q \qquad (1.2.12)$$

Where:

i – symbol of ice drift velocity vector component on coordinate axis (x, y) and corresponding polynomial coefficients;

X, Y – coordinates of drift vectors $\vec{V}$ beginning;

m – degree of polynomial by argument p;

t – degree of polynomial by argument q;

a_{pq} – polynomial coefficient.

These patterns show the Transarctic Ice Flow that moves toward the Greenland Sea between the near-pole region and the northern margins of the Eurasian shelf seas. Large quantity of ice exported from the Russian Arctic Seas joins this flow on the left, while the anticyclonic gyre area with its center approximately at 78^0 N, 150^0 W, adjoins it on the right. Seasonal changes are well observed in these patterns.

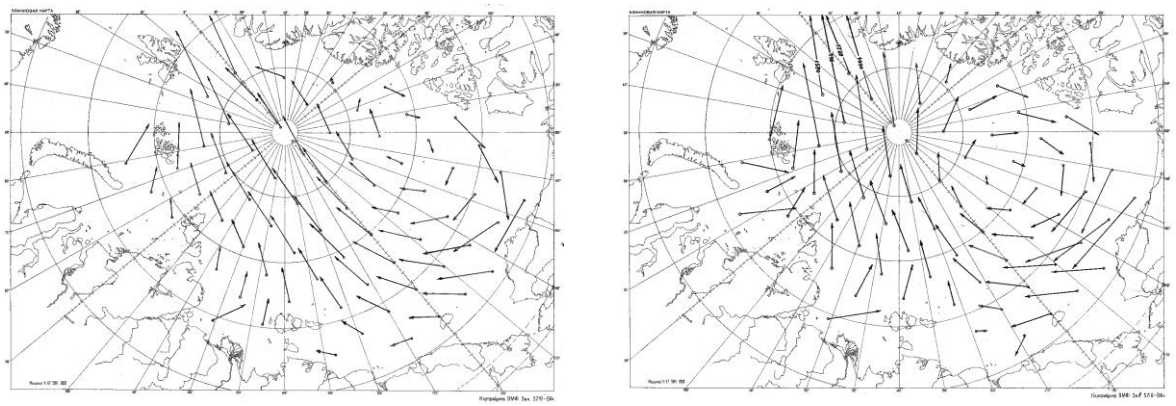

Fig. 1.2.8 – (а) – Scheme of resultant ice drift for April-September; (б) Scheme of average resultant ice drift for October-March

Ice entrained by the Transarctic Flow from the Kara Sea is exported to the Greenland Sea in 1-2 years, from the Laptev Sea – in 2-3 years, from the East-Siberian Sea – in 3-4 years, and from the Chukchi Sea – in 4-5 years. The period of ice circulation within the anticyclonic gyre changes from 4 to 10-12 years.

These schemes are used for climate forecast of different objects motion for long time periods.

1.2.3. Modelling of sea ice dynamics

Modelling of sea ice dynamics is based on consideration of force balance equation, which influence ice cover, called Equation of motion. In its basis – application of second Newton's law to ice dynamics: resultant value of all forces, effecting ice cover area unit, is equal to ice mass production, related to this area, on acceleration, i.e.

$$\rho_{л} H \frac{d\vec{V}}{dt} = \vec{\tau}_a + \vec{\tau}_w + \vec{C} + \vec{G}_n + \vec{G}_t + \vec{R} \qquad (1.2.13)$$

Where: $\rho_{л}$, H – ice density and thickness;

$\vec{V}$ – drift velocity vector;

τ_a, τ_w – tangent stresses on upper and lower ice surfaces;

$\vec{C}$ – Coriolis force;

$\vec{G}_n$ – gravity projection to sea surface;

$\vec{G}_t$ – horizontal component of tide-generating force;

$\vec{R}$ – force of internal interaction.

Estimations of relative force values, included into equation (1.2.13), significantly depend on average velocities, and, therefore, on motion scale.

In these models for solving equation (1.2.13) the components, composing this equation, are expressed by dependences, based on physical laws (mechanical). As a rule, such dependences include different parameters, which are defined in natural or laboratory experiments.

Models of ice cover dynamic differ by both degree accounting of acting forces and way of their expressing. In earliest models ice cover was considered as a level endless plate, to which spatially invariable tangential forces (τ_a и τ_w) and Coriolis acceleration were subjected Fig. 1.2.9). In models of next level ice cover was considered to be a viscous liquid film, located between two layers of less viscous liquids – air and water. Thereby internal interaction force is connected with irregularity of ice drift velocity field in these models.

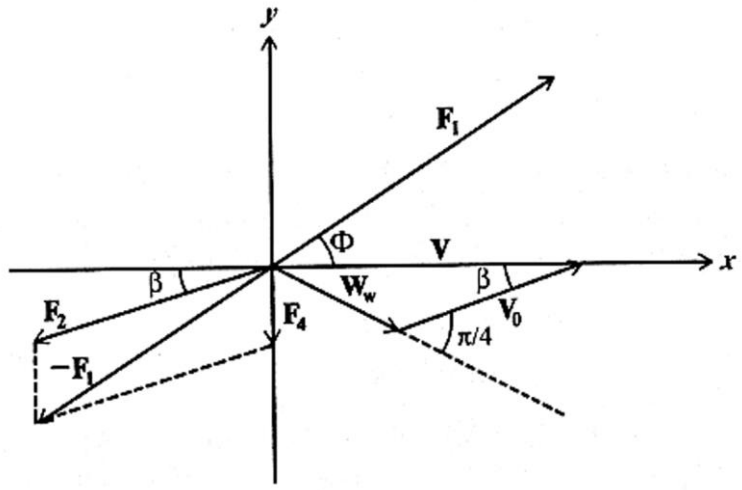

Fig. 1.2.9 – Scheme of ice drift velocity and force directions according to Shuleikin V.V.

First term of right part of equation (1.2.13), expressing tangential wind stress, is determined through vertical gradient of average wind velocity:

$$\tau_a = \rho_a k_a \frac{\partial W}{\partial z} \qquad (1.2.14)$$

Under logarithmic wind profile, which is typical for atmosphere surface layer, this formula is transformed as:

$$\vec{\tau}_a = \rho_a c_a |W|\left(\vec{W}\right) \qquad (1.2.15)$$

Here coefficient c_a is function of aerodynamic roughness z_0, of Karman constant and height of wind observation.

Tangential tension on lower ice surface (τ_w) is usually determined in the same way as τ_a:

$$\tau_w = \rho_w c_w |V_r| \vec{V}_r \qquad (1.2.16)$$

where: ρ_w – water density;

c_w – dimensionless impedance coefficient.

Calculations are complicated by circumstance that value V_r – relative velocity, which is equal to geometrical difference in vectors of drift velocity and current on lower boundary of water sublayer, where tangential drag stress changes weakly in vertical direction.

Standard expressions are used to determine third and fourth terms in equation of motion. Coriolis force, presenting horizontal projection of Earth rotation deflecting force, is given by:

$$\vec{C} = \rho_л Hf \times \vec{V} \qquad (1.2.17)$$

where: $f = 2\omega \sin\varphi$ – Coriolis parameter;

ω – angular velocity of Earth rotation;

φ – geographical latitude.

Coriolis force is directed at right angles to the right (in northern hemisphere) to the direction of ice drift velocity V. Gravity force projection to sea surface G_n is given by formula:

$$G_n = -\rho_л g H \nabla\zeta \qquad (1.2.18)$$

where $\nabla\zeta$ –tilt of level sea surface.

In most works, while determining forces of internal interaction in ice cover, expressions, similar to relations used in mechanics of continua, were used. In this case interaction force is divergence of internal stress tensor (σ_{ij}):

$$\frac{1}{H} R_i = \frac{\partial \sigma_{ij}}{\partial x_j} \qquad (1.2.19)$$

For determination of force R it is necessary to establish determinant equation, connecting internal stress tensor with parameters of ice cover conditions or with ice drift characteristics.

Among many works, describing sea ice evolution, there are models, describing viscous, elastic, plastic and also combined viscous-elastic, elastic-plastic or viscous-elastic-plastic properties of ice cover.

During development of ice dynamics models, it is necessary to take into account, that ice cover differently react to tangential and normal stress, to tensile and compression strain, that can simultaneously exist under ice motion. Forces of internal interaction depend on ice cover condition – its thickness, concentration, strength, forms, and also on occurrence and orientation of leads (cracks, channels) in compact ice.

Dynamic-thermodynamic models of ice cover evolution allow calculating kinematic changes of ice cover parameters. Calculations are based on differential equation, which is a result of mass conservation law. Specifically, for function of ice cover concentration it is given by:

$$\frac{\partial N}{\partial t} = -div(N\vec{V}) + SN \qquad (1.2.20)$$

Where: $0 \le N \le 1$ – function of ice cover concentration;

S_N – thermodynamic term.

To calculate advective changes of parameters, which do not depend on velocity divergence (e.g., level ice thickness, H), the following equation is used:

$$\frac{\partial H}{\partial t} = V_x \frac{\partial H}{\partial x} + V_y \frac{\partial H}{\partial y} + S_H \qquad (1.2.21)$$

where S_H – thermodynamic term.

If during calculations it is found that in any grid point $N > 1$, velocity field is corrected by means of iterations, and ice thickness correction is calculated (due to ridging). Correction is added to average (for grid point) ice thickness. The way of expressing internal resistance force in main ellipse deformation axis (only normal forces are subjected) with taking into account deformation sign - is interesting aspect to mention. Reasonable definition of boundary conditions has the main importance in ice cover models.

1.2.4. Regularities of ice cover irregular motion

In studies of ice cover motion, apart from translation ice motion – actually drift, effects, which occur from changes of motion velocity in space and time, have great practical and science interest. These changes are determined by ice drift velocity field.

1.2.4.1. Irregular motion types

At any moment components V_x и V_y of velocity vector V are functions of coordinates x and y, i.e. $V_x = V_x(x, y)$, $V_y = V_y(x, y)$.

Having chosen origin of coordinates in arbitrary point x_0 and y_0, we develop these expressions in Taylor series (high-order terms are discarded):

$$V_x = V_{xo} + (\frac{\partial V_x}{\partial x})x + (\frac{\partial V_x}{\partial y})y$$
$$V_y = V_{yo} + (\frac{\partial V_y}{\partial x})x + (\frac{\partial V_y}{\partial y})y \qquad (1.2.22)$$

From four spatial derivatives, contributing to equation (1.2.22), the following four characteristics of plane motion irregularity can be obtained:

$$div\vec{V} = \frac{\partial V_x}{\partial x} + \frac{\partial V_y}{\partial y} \qquad \textit{(divergence)} \qquad (1.2.23)$$

$$rot\vec{V} = \frac{\partial V_y}{\partial x} - \frac{\partial V_x}{\partial y} \qquad \textit{(rotor)} \qquad (1.2.24)$$

$$def_1\vec{V} = \frac{\partial V_y}{\partial x} + \frac{\partial V_x}{\partial y} \qquad \textit{(angular deformation)} \qquad (1.2.25)$$

$$def_2\vec{V} = \frac{\partial V_x}{\partial x} - \frac{\partial V_y}{\partial y} \qquad \textit{(linear deformation)} \qquad (1.2.26)$$

It's not complicated to prove, that expression

$$def\vec{V} = \sqrt{(def_1\vec{V})^2 + (def_2\vec{V})^2} \qquad (1.2.27)$$

is invariant relative to coordinative system. That is why equalities (1.2.22) can be written as follows:

$$V_x = V_{x0} + \frac{x}{2}div\vec{V} + \frac{x}{2}def\vec{V} - \frac{y}{2}rot\vec{V}$$
$$V_y = V_{y0} + \frac{y}{2}div\vec{V} - \frac{y}{2}def\vec{V} + \frac{x}{2}rot\vec{V} \qquad (1.2.28)$$

Cinematic nature of expressions (1.2.28) is that ice cover can be transferred from one location to another by means of translation (actually drift), divergence (i.e. diverging and compacting), deformation (in restricted sense this term means that body shape changes without changing size) and, finally, rotation. Common for motion, described by last three terms, is its typical spatial irregularity of velocity field. That is why, formulas (1.2.23 – 1.2.26) can serve as kinematic indicators of ice cover motion irregularities, each of them expresses rather definite and independent from each other irregularity features.

Velocity of ice cover rotation changes with time; its average value depends on time scale, season; it decreases with increase of ice cover concentration and increase with reduction of ice floes size.

It is known, that rotation velocity in continuum medium is connected with characteristic of cross irregularity of velocity - rotor (vorticity) as:

$$\frac{\partial \omega}{\partial t} = -\frac{1}{2} rot\vec{V} \qquad (1.2.29)$$

Studies of ice cover rotary motion have not only scientific, but also large practical interest. Data about ice floe rotation allow to judge about occurrence of cross irregularity of wind and gradient ice drift. Orientation of devices, put in the ice, is changed as a result of rotation, etc. Using listed relations between ice drift velocity and gradient of atmosphere pressure, we get:

$$\text{rotV} \approx \text{k rotW} \approx K\nabla^2 P \qquad (1.2.30)$$

Where ∇^2 – 2D Laplace operator.

Consequently, wind component of ice motion velocity rotor (and also velocity of ice cover rotation) is proportional to wind velocity rotor or atmospheric pressure Laplacian. Analysis of numerous observation data confirms validity of dependence (1.2.30).

Divergence of ice drift velocity, as shown before (1.2.20), is closely connected with changes of ice cover concentration. This formula can be written as follows:

$$\frac{\partial N}{\partial t} = N \quad , \quad div\vec{V} - \vec{V}\, grad\ \text{N} \qquad (1.2.31)$$

The first term of right equation part characterizes changes of concentration due to spatial irregularity of ice drift velocity, and the second – changes of concentration due to advection. divergence of ice motion velocity can be caused by the following reasons:

- spatial irregularity of currents velocity and sea level;

- spatial irregularity of wind fields;
- coast influence (or motionless ice);
- ice cover heterogeneity (its thickness, concentration, hummocking, on which upper and lower ice surface roughness, and also mass, for surface unit, depends);
- processes of horizontal diffusion;
- non-stationarity of external influence;

Velocity divergence, caused by tidal currents, depends on type, height and length of tidal wave. In case of progressive wave, divergence maximum (i.e. the largest intensity of ice cover diverging) is observed at the moment, when tidal current is changed to ebb current. In contrary, the largest converging (the largest intensity concentration increase, and with N=1- the largest compacting) must occur at the moment, when ebb current is changed into tidal. At that ice cover concentration reaches its maximum on the wave crest (high water) and minimum - at the moment of tidal current (low water). Amplitude of tidal changes of divergence under other equal conditions increase with the wave length decreasing, depended on wave period and sea depth. That is why tidal phenomena in ice cover, normally noticeable on shelf, are insignificant in deep sea.

Numerous studies show that divergence of ice drift velocity, caused by wind field irregularity, provides the major contribution in the mechanic change of ice cover concentration far from coast and ice edge. At that, both wind field irregularity and deviation of wind drift from isobaric (geostrophic) relations are important, because under isobaric ice drift divV = 0.

The listed relations between drift velocity components, wind and pressure gradients should be used to find connection of ice motion velocity divergence with wind and pressure fields. Thus we get:

$$div\vec{V} = \frac{k\sin\beta}{\sin\gamma} div\vec{W} = K\sin\beta\nabla^2 P \qquad (1.2.32)$$

The model of stationary pressure field, suggested by D.A. Drogaitsev, should be used to find out dependence of drift velocity divergence and sea ice concentration redistribution on wind fields irregularity. Such field can be described by expression:

$$P = P_o \sin\frac{2\pi}{L_x} x \sin\frac{2\pi}{L_y} y \qquad (1.2.33)$$

Where: P –deviation of atmospheric pressure from some average;

P_o – amplitude of pressure changes;

L_x, L_y – distance parallel to coordinative axis between maximum and minimum of atmosphere pressure.

View of this field under P_o =10 мб. and L_x= L_y = 4000 km is shown on Fig. 1.2.10

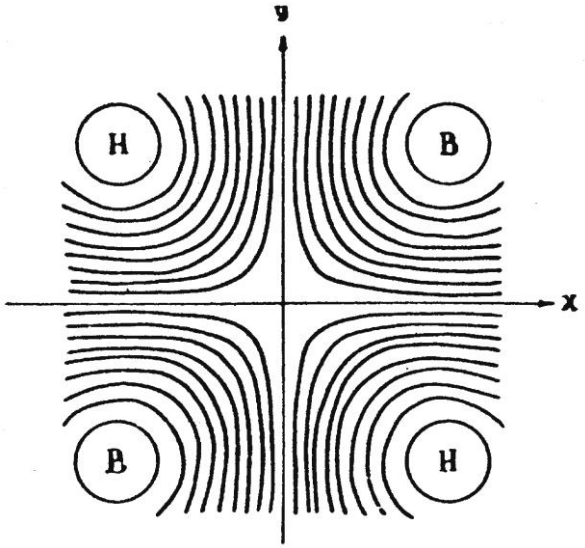

Fig. 1.2.10 – Scheme of pressure field, according to Drogaitsev D.A. (isobars – through GPa)

Ice drift components were calculated from formulas (1.2.11) with $\beta=20^o$ taking into account empiric dependence of isobaric coefficient value K from gradient of atmosphere pressure. Ice concentration was calculated by using the equation (1.2.31).

Calculations results of concentration redistribution in pressure field for 10-day periods under even initial concentration, equal to 8/10-th are shown in Fig. 1.2.11. As it is seen from the figure, small changes of concentration occur close to cyclones centers (depression) and anticyclones (compaction). On axis of deformation field these changes are not large; therefore, role of nonlinearity of ice drift velocity dependence on pressure gradient has the second importance. There aren't any concentration changes in hyperbolic field point.

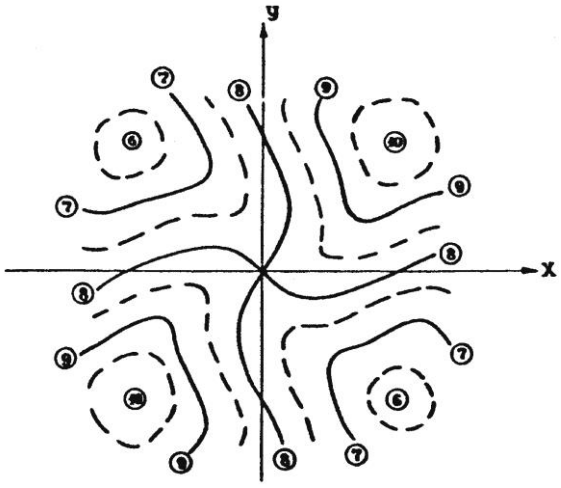

Fig. 1.2.11 – Calculated distribution of ice cover concentration in stationary pressure field (Fig. 1.2.10) with T_0=0,8 (8/10-th) after 10 days

Nature of ice concentration changes, revealed in the listed calculation results, is confirmed by numerous air reconnaissance observations. In years, when cyclonic fields dominate in summer above the Arctic Basin, observers noticed significant ice cover divergence, reaching sometimes 4-6/10-th. In contrary, in years, when frequency of occurrence of arctic cyclone increased, ice cover was compact. Results of triangles and quadrangles area calculations, built according to simultaneously measured coordinates of Russian and American drifting stations and to observations from special polygons, can be considered as confirmations of these regularities.

Distribution of ice drift velocity divergence, areas of ice concentration increase and diverging in stationary baric systems was considered before. However, a number of dynamic effects is connected with non-stationarity of pressure fields – their motion in space and changes in time. Processes in moving baric systems, leading to ice concentration increase, are observed in front of cyclone, and diverging– in front of anticyclone.

It is known, that heterogeneity of ice cover thickness, and also roughness of its upper and lower surfaces, mostly depending on hummocking, cause spatial irregularity in velocity of ice drift, leading to internal strains and deformations. Large-scale heterogeneity of ice thickness is mostly noticeable in seas, where ice is transported out. There ice cover becomes gradually younger, and well-marked gradient of ice thickness occurs, directed from thick first-year ice to flaw polynyas, which in winter are rapidly covered with young ice. Large horizontal gradients of ice thickness are also observed close to multiyear ice boundary. Significant heterogeneity of hummocking can be found near external fast ice boundary in conditions, when pushing drift is dominant, and also in region of strongly broken ice, survived after summer melting.

Ice cover deformation, as divergence, takes place under occurrence of spatial heterogeneity of ice cover velocity motion. Dependence of deformation velocity on wind irregularity (pressure field) can be easily found, by substituting expressions (1.2.11) in formulas (1.2.23), (1.2.24) and (1.2.26).

$$def\vec{V} = K\sqrt{\left(\frac{\partial^2 P}{\partial x^2} - \frac{\partial^2 P}{\partial y^2}\right)^2 + \left(2\frac{\partial^2 P}{\partial x \partial y}\right)^2} \qquad (1.2.34)$$

As it is seen from this formula, maximum value of deformation velocity doesn't depend on angle between ice drift directions and geostrophic wind (β), but is determined only by isobaric coefficient value and pressure field peculiar features. Using equation (1.2.33) for description of last expression, distribution of value $def\vec{V}$ can be obtained (Fig. 1.2.12) in deformation pressure field similar to one shown in Fig. 1.2.10. In contrast to the last one L_y/L_x=0,7 was taken, i.e. it is rather stretched along *x* axis.

Analysis of formula (1.2.34) shows, that deformation value, taken into account by first term of radicand, is maximum in pressure centers and equal to zero in neutral lines of pressure field. If $L_y=L_x$ this term turns into zero, consequently, in pressure systems, close to circle, this component of deformation velocity is practically absent. Component, described by the second term of radicand (1.2.34), reaches its maximum value in hyperbolic points of pressure fields and equal to zero in centers of cyclones and anticyclones and along lines, connecting neighbor centers.

From Fig. 1.2.12 it is seen, that under moderate "elongation" of pressure systems region of maximum deformation is located in area of baric saddle, whereas in centers of cyclones and anticyclones deformation is not large. Obtained result explains regularity, known from observations: the strongest ice shearing – breaking and hummocking – are observed in areas of baric saddles, for which weak wind is typical.

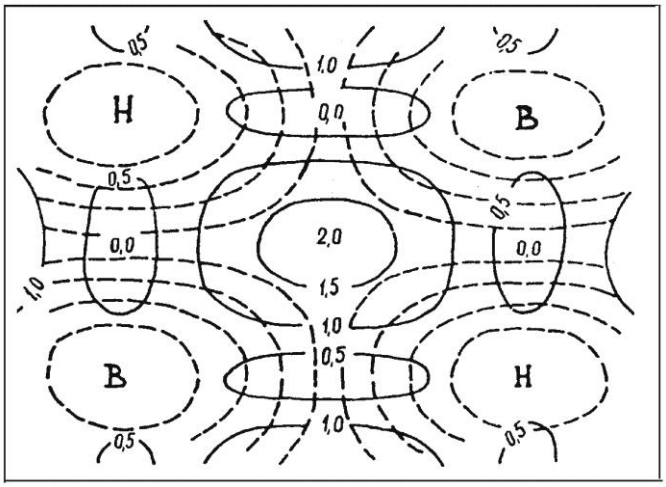

Fig. 1.2.12 – Distribution of deformation values (in 10^{-7} c^{-1}) in pressure field

For visual presentation of deformation for any time period (or deformation velocity) it is convenient to make deformation ellipse (deformation velocity). Direction of longer ellipse axis corresponds to maximum elongation (or minimum pressure), small axe – minimum elongation (maximum pressure). From the deformation ellipse we can approximately judge about cracks direction in ice cover. Normally direction of cracks in ice cover is perpendicular to longer axis of deformation ellipses. These regularities explain typical systems of leads in sea ice cover, and other arched systems, observed while approaching to straights.

Taking into account dependence of velocities divergence and deformation from heterogeneity of ice thickness and hummocking, it can be summarized, that cracks mostly form along isolines of equal thickness, leaving thicker ice from the right, if the wind blows along these isolines. This regularity is confirmed by data of air reconnaissance: in seas, where ice thickness increases from south to north, wide leads often form in ice cover with winds of eastern quarter. Characteristic

features in ice cover deformation, connected with drift irregularity, occur also close to barriers (land, fast ice, etc). Concentric system of cracks, which is often seen in region of anticyclonic water and ice circulation northwards of the Beaufort Sea, points to significant role of sea level tilt in this region.

Thus, by means of mathematical modeling it was possible to explain, and in some cases even to predict appearing of many features in ice cover distribution, which are important for implementation of transport and other operations in sea ice cover.